Egypt. J. Chem. **Vol. 66**, No. 9 pp. 375 – 384 (2023)

Egyptian Journal of Chemistry

http://ejchem.journals.ekb.eg/

Green Synthesis, Dielectric Constant and Electrical Conductivity Studies of Nano Sized CoMnFe System

N. M. Deraz[1], H.M. Shokri[2*], A. H. Salama[1] and S. A. Abou El-Enein[3]

[1] *Physical Chemistry Department, National Research Centre, Dokki, Egypt.*

[2] *R&D Chemist at El-Nasr Company for Intermediate Chemicals (NCIC Abou Rawash), Giza, Egypt.*

[3] *Chemistry Department, Faculty of Science, Menoufia University, Egypt.*

Abstract

A Series of nanosized $Co_{0.3}Mn_{0.7}Fe_2O_4$ system was prepared by using combustion method with different amounts of white egg as biofuel. The structural and morphological characteristics of the as prepared system were achieved by using XRD and TEM techniques. The optical and electrical properties of the as synthesized system were determined. The results showed that CoMnFe solids have nanocrystalline phase with a cubic spinel structure. TEM study revealed that the average particle size of the previous system ranged in nano scale. Additionally, the electric properties such as direct current electrical conductivity, alternating current electrical conductivity and dielectric constant were studied in the frequency range from 42 Hz to 1MHz with a temperature range from room temperature up to 125°C.Various results were set to determine the optimum content of biofuel to have system with maximum capacity to be used as a candidate for electrodes on super capacitor applications.

Keywords: XRD,TEM, UV- Vis Spectra, Dielectric constant, and Ac- electrical conduction mechanisms

1. Introduction

Transition metal oxides present an attractive alternative as a super-capacitor electrode material because of their high specific capacitance at low resistance. Moreover, it is easy to construct high energy, high power super-capacitors. Among these oxides that use as an electrode material for super capacitors applications are manganese, cobalt and iron oxides [1-31]. Indeed, the theoretical capacitance of manganese oxides reaches 1100 Fg^{-1}due to highly complex of these oxides with different valance states. However, the electrochemical reversibility of the redox transition of manganese dioxide (MnO_2) is usually too low to be applicable due to poor capacitive response depending upon its high resistance. On the other side, most of the manganese oxides reported in the literature showed specific capacitances as high as 600 $Fg^{-1}$for thin films, 150-300 $Fg^{-1}$for powder-based electrodes in aqueous electrolytes and 400-621 $Fg^{-1}$for amorphous electrolytic manganese dioxides and MnO_2 –based mixed oxides [1-5]. However, because of their environmental friendliness, low cost, availability of polymorphs, and wide range of uses, iron oxides are seen to be promising materials. [6-20].Hematite (α-Fe_2O_3) and magnetite (Fe_3O_4) are the major sources of iron in industrial metal iron production processes. It was recorded that the effectiveness of both α-$Fe_2O_3$and Fe_3O_4 as electrode materials in super capacitor applications depend on their crystalline, phase purity and morphology [21]. But, α-Fe_2O_3 has received less attention than Fe_3O_4 primarily because to its substantially poorer conductivity [22].In addition, cobalt oxides (CoO, $Co_2O_3$and Co_3O_4) are another battery electrode material that has been studied for super capacitor applications. This family of

*Corresponding author e-mail: rodyshokri412009412009@gmail.com.; (H.M. Shokri).
Received date.2022-10-22; revised date 2022-12-05; accepted date 2022-12-25
DOI: 10.21608/EJCHEM.2022.170246.7113

materials displays a charge transfer process similar to batteries and a current-voltage response similar to a double layer capacitor. The spinel Co_3O_4 oxide is the one that has been examined the most for use in electrochemical capacitors. [23-31]. Alternatively, it was found that the co-existence of various elements in the crystal structure of the investigated material brought about different cations containing various electrons with modification in the magnitude of electrical conductivity. So, the complex chemical composition of metal oxides is the subject of several studies because the individual metal oxides were deemed unable to fully meet the overall performance needed for super capacitor electrode. It was found that The electrical conductivity of the spinel $NiCo_2O_4$ materials is two to three orders of magnitude greater than that of the individual metal oxides comprising NiO or Co_3O_4[32-34]. In addition, doping of Co_3O_4 by NiO enhances the electrical conductivity from 3.1 $*10^{-5}$ to 0.1-0.3 Scm^{-1} [35].The previous results showed that the inclusion of more than one metal oxide would allow for higher electrochemical activity depending upon the variety and valence of metal ions. Additionally, In comparison to single metal oxides, the synergistic impact between various species of mixed oxides would improve the overall performance of individual metals and promote their activities as ion adsorption, diffusion, and transport compounds. From this point of view, our tendency was to prepare mixed ferrites containing Mn and Co by using an easy, simple and environmentally friendly method. However, ferrite-based nanoparticles have major applications such as energy storage, gas sensor, electronic materials, and catalysts. In addition, ferrite powders are used in the coatings of **tapes. Mn** and/or Co ferrites are among of the most adaptable spinel-type ferrites due to their wide range of possible uses. Cobalt ferrite with a cubic spinel structure, $CoFe_2O_4$ ($CoO•Fe_2O_3$), is a well-known and significant family of iron oxide materials which are thermally and chemically stable [36]. However$CoFe_2O_4$, which falls between soft and hard magnetic materials, is a semi-hard substance. It is therefore employed in magneto-strictive devices like sensors and actuators.

2. Because of its strong coercivity at ambient temperature, mild saturation magnetization, high dc electrical resistivity, and low dielectric losses, $CoFe_2O_4$ nanoparticles have a wide range of applications [37, 38]. For high frequency applications, Mn ferrite provides excellent mechanical and chemical stability as well as little power loss. They are known as soft ferrites and have a poor conductivity. Spinel ferrites have been produced using a variety of techniques, including solid-state reactions, high-energy ball milling, sol-gel, hydrothermal synthesis, co precipitation, combustion synthesis, micro-emulsions, and microwave hydrothermal procedures [39–41]. Combustion-based production of different ferrites is a particularly straightforward, secure, and quick manufacturing approach that results in homogenous, high-purity, and nanocrystalline ceramic powders .In previous work, one of the authors prepared the ferrite-based material using an auto combustion method based on egg white as fuel, relying on a number of benefits of this approach, including the absence of intermediate decomposition, the maintenance of high stoichiometry of the product with the subsequent easily controlled particle size of the product, excellent mixing of starting materials, chemical homogeneity, molecular level mixing, and the tendency of partially hydration.This work aims to study the effects of egg white contents as biofuel on the fabrication, morphology and electrical properties of the as synthesized solids containing and $Co_{0.3}Mn_{0.7}Fe_2O_4$.The structural properties and the band gap energies for the as synthesized solids were determined by using XRD and UV-Vis spectra, respectively. Finally, the variation of dielectric constant with frequency at different temperatures was studied in detail.

2. Expermintal

2.1. Materials

On a hot plate, the calculated amount of Mn Nitrate, Co Nitrate and Fe nitrates were mixed with a definite amount (5 ml) of egg white, then the final mixture was heated at 70℃ until gel appears. The temperature of the as prepared mixture was raised to 250℃ and kept it for 8-15 minutes to evaporate the water crystals. During this process sparks appeared, and foam appear in one corner, giving a brownish superfine massive product containing $Co_{0.3}Mn_{0.7}Fe_2O_4$ nanoparticles.

This process repeated at different concentrations of biofuel (10 ml and15 ml). Indeed, the samples were mentioned in this text as S1,S2 and S3 respectively. The following scheme gives an illustration for the preparation of the previous samples.Aldrich Company provided the previous nitrates. These were quantitative reagents that were applied without further refining. Raw egg from surrounding chickens was used to extract the egg white.

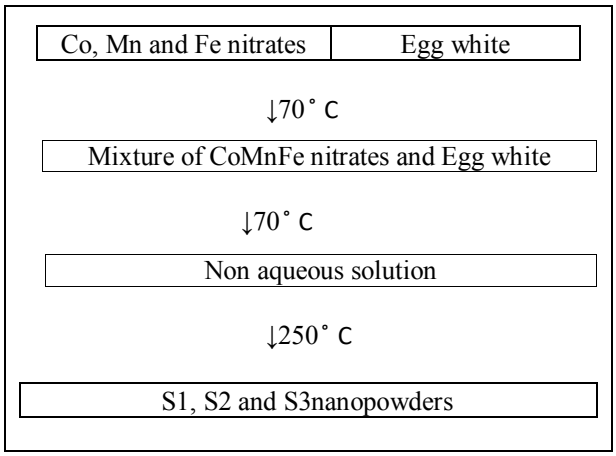

The proposed scheme for the preparation of S1, S2 and S3 solids

2.2. Techniques

2.2.1.X-ray powder diffraction patterns (XRD)

A Philips diffract metre (model pw 1051) was used to perform X-ray powder diffraction patterns (XRD) at room temperature while utilizing Ni filtrated Cu K. Radiation (, 1.5404 A°). Scherer's equation was used to estimate the size of the crystallites in the crystalline phase that was present

$$L = (K\lambda)/ (\beta \cos\theta) \qquad (1)$$

Where λ is wavelength of x-ray beam used, K is the geometrical Scherrer constant equal to 0.94 which is related to crystalline shape, β is peak width at half maximum height. the value of β in the 2Θ axis of diffraction profile must be in radius. the Θ is Bragg angle and can be in radius since the cosΘ corresponds to the same number.

2.2.2. UV-Vis spectroscopy

UV-Vis spectroscopy was used to characterize the optical absorption properties of the prepared compounds. Absorption spectra were recorded in the wavelength range of 190 to 800 nm using a JASCO V360 UV-visible spectrometer. All spectra were recorded at room temperature.

2.2.3. Transmission Electron Microscopy (TEM)

Transmission electron microscopy (HR TEM-JEM 2100, JEOL, Japan) was used to examine the shape and particle size distribution of the produced compounds at 200 kV accelerating voltage. The samples were made by dissolving the powder in 100% ethanol in an ultrasonic water bath. The suspension was then dropped into the carbon grid and allowed to dry.

2.2.4. Electrical characterization

Using the HICKI-LCR-Hi Tester (3532-50), dielectric and electrical conductivity tests have been made over the frequency range of 50 Hz to 5 MHZ and the temperature range of 0 °C to 125 °C. Using a hydraulic press, the ferrite samples for this study were compressed into cylindrical pellet forms with a diameter of 10 mm and a thickness of roughly 12 mm. The disc containing the test samples is positioned between the LCR meter's two electrodes. A single voltage level of 0.02 v was maintained.

3. Results and discussion

3.1. XRD investigation

The effect of biofuel concentration on the crystal structure of the prepared nano- composites was studied by XRD- diffraction pattern represented in Fig. 1. This figure ensures that the synthesized samples composed of CoMn ferrites ($Co_{0.3}Mn_{0.7}Fe_2O_4$).The *XRD patterns revealed that* $Co_{0.3}Mn_{0.7}Fe_2O_4$ powders crystallize with a cubic structure and the space group *Fm3m*, which well matched with the reported values in JCPDS files (No. 22-1086 and No. 74.2403).

Fig. 1 shows XRD patterns ofS1, S2 and S3 Samples. it can see from the figure that the formation of Co Mn ferrites increases as fuel content increase. The maximum formation of the ferities was observed in S2 samples. However, XRD pattern confirms that the as prepared samples consist entirely of $Co_{0.3}Mn_{0.7}Fe_2O_4$ as single face with a good crystalline. The crystallite size of S1, S2 and S3 were calculated by using Scherer equation are 20, 15 and 10 nm respectively.

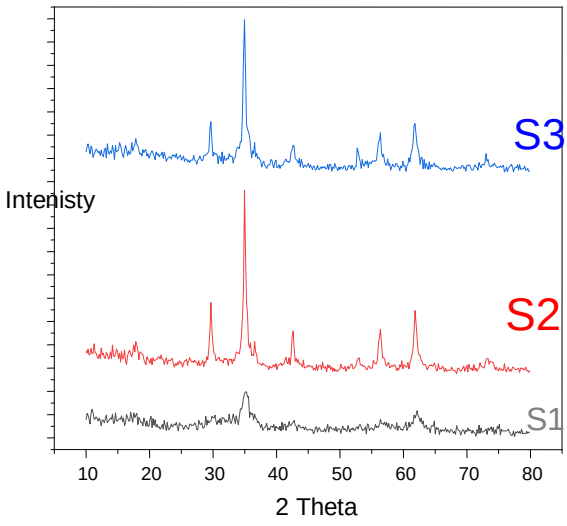

Fig (1): XRD-pattern for S1, S2 and S3 samples

3.2. Morphology

Transmission electron micrograph (TEM)images of $Co_{0.3}Mn_{0.7}Fe_2O_4$solid prepared by using 10 ml egg white assisted combustion technique (S2 sample) shows in Fig. 2a. The calculated inter planar spacing values confirm that the samples consisted of nanoparticles metal oxides with cubic structures which is compatible with XRD data. The average particle size of the investigated sample ranged from 10 to 15 nm. Indeed, the morphology of metal oxide is very important as It has to do with a certain surface area, diffusion paths, surface to volume ratios, and consequently the performance of the super capacitor. Numerous research projects concentrated on different metal oxides with diverse morphologies, including porous thin films, nanowires,nanorods,nanotubes, nanoflowers, hollow spheres, and nanopillar arrays. Additionally, the morphologies of metal oxide-based super capacitors have a significant impact on their electrochemical properties with high specific surface area and porous nanostructures.

TEM technique enabled us to study the selected areaelectron diffraction (SAED, the inset of Figure 2b) for the S1, S2 and S3 samples.Fig. 2b shows a set of concentric rings for the S2 sample, indicating the formation of polycrystalline structure.

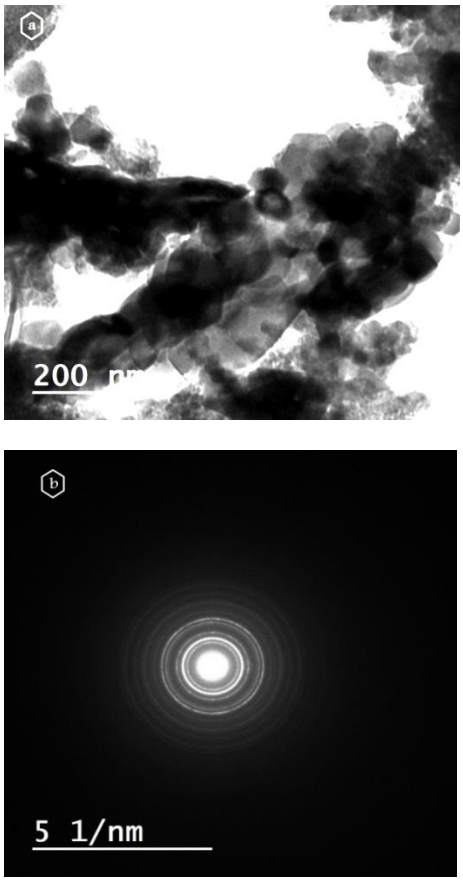

Fig. (2): the TEM analysis of S2 sample, (a) TEM images and (b) SAED

3.3. Optical properties

The optical absorbance of the prepared solids was derived from the transmission and reflection measurements in the ultraviolet-visible (UV-Vis) wavelength regime. Considering the indirect optical transition in the material.

The optical band gap energy (E, eV)of various ferrites containing $Co_{0.3}Mn_{0.7}Fe_2O_4$ can calculate by using the following Tauc's equation[42].

$$E = h\,(c/\lambda) \qquad (2)$$

Where, C is the speed of light 3.0×10^8 m. s^{-1}, h is the Planks constant 6.6 $x10^{-34}$J. s, and 1 eV = 1.6×10^{-19} J. The cut-off wavelength (λ) is calculated by the extrapolation of the linear portion of the relation between the absorbance and wavelength.

The UV-electronic spectra of the S1, S2 and S3 samples are graphically represented in Fig. 3 which reveals that the maximum wavelengths of the spectral bands affected by the concentration of the biofuel used. All the samples have a strong broad maximum ranged from 220 to 600 nm. It is clear to notice that the broad absorption band around 475 nm which is assigned to the transition$6A_{1g}$ (s)→$4T_{1g}$ (G) of Mn^{2+} ions [43]. The recorded band gap values could be referred to the increase of electronic (charge) density because of incorporation of transition metal ions of Co and Mn which possess different oxidation states. The increase of charge density could overlap with electron clouds of central Fe particles thus; up-shift in energy level of the valence band electrons of Fe atom could be attained. The values of band gap energy were found to be 1.4, 1.5 and 1.4eV for S1, S2 and S3 respectively.

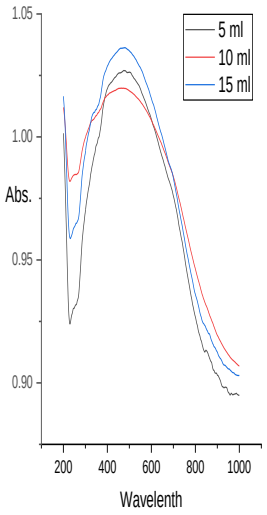

Fig. (3): UV-Vis spectra of S1, S2 and S3 samples

3.4. Electrical conductivity studies

Electrical conductivity of a semiconductor is a temperature dependent process resulting from orderly motion of weakly bounded charged particles under the action of an applied electric field. Indeed, the most important property of the semiconductor nanoparticles depends on charge carriers such as cations/anions or electron holes that lead to conduction process as a function of frequency and temperature.

3.4.1. AC-conductivity studies

Fig.4 displays the dependence of ac-electrical conductivity of various $Co_{0.3}Mn_{0.7}Fe_2O_4$ samples on frequency at different temperatures; in frequency range 40 HZ to 5MHZ at a temperature varying from room temperature to 125 ^{o} C.

In fact, the ac-electrical conductivity (σ_{ac}) was calculated from the measured resistance at the same temperature and frequency range. The conductivity was calculated using the relation

$$\sigma_{ac} = La/R_p \qquad (3)$$

where, R_p is the sample resistance, a is the cross-sectional area of the sample, and L the sample thickness.

From Fig. 4, two points are considered: (i) a plateau at low frequency region which is related to dc-conductivity (σ_{dc}) (ii) the high frequency corresponds to a bulk relaxation phenomenon that resulted from migration of trapped ions related to ac-conductivity [44]. These values for all samples increase with an increase of both frequency and temperature, showing that the most probable mechanism for conduction of $Co_{0.3}Mn_{0.7}Fe_2O_4$ nanoparticles is a hopping conduction mechanism [45]. It is also observed that as the concentration of biofuel increases from 5 ml to 10 ml, the value of σ_{ac} increased by one order after the increase of concentration of biofuel results in a decrease in the value of ac-conductivity.

Moreover, the ac-conductivity was very sensitive to frequency above 200 HZ and the dependency increased further at high temperature Fig. 4. The frequency width of the plateau region (dc)as well as the magnitude of ac conductivity increased with increasing temperature. The frequency dependent region showed a regular tendency and shifted to higher frequency; similar activity was reported previously on different semiconductor types [46]. This behavior can be attributed to the presence of numerous dielectric relaxation processes and thermally activated charge carrying species in $Co_{0.3}Mn_{0.7}Fe_2O_4$ nanoparticles. It is also observed that ac-conductivity has the highest value when 5 ml of biofuel was used.

The dependency of the AC-conductivity at high frequencies obeys the Janscher's power law as follow:

$$\sigma_{ac} = A\omega^{s} \qquad (4)$$

where: A is a constant that depends on the strength of polarizability, ω is the angular frequency and s is the fractional exponent which represent the degree of interaction between the mobile ions and the surrounded environment [47].

The " S " values are obtained from the slope of linear fitting plots of log (σ) vs. log f depending upon the illustrated data in Fig. 4. The behavior of frequency exponent " S " with temperature is graphically represented in Fig. 5. It is observed that the frequency exponent decreases with increasing temperature for S1 and S2 where for S3 is almost unchanged till 100^{O}C after which it began to increase with temperature. The s values are found to vary from 0.488, 0.578 and 0.252, to 0.25, 0.158 and 0.294 for S1, S2 and S3, respectively, within the experimental temperature range. This behavior agrees well with the correlated barrier hopping (CBH) model. According to this model, the electrical conduction occurs through the hopping of mobile charge carriers over the coulomb potential barrier between two defect centers. Also, the value of S describes the interaction existing between the mobile ions with their surroundings molecules during conduction. On increasing the biofuel concentration there is a decrease in " S " values resulting from the decrease in interaction between C atom (resulted from combustion of biofuel) and their neighboring sites and thereby give rise to an increase in ionic mobility, which in turn increases the ionic conductivity. This behavior was more pronounced in case of the S3 sample due to an increase of the content of C carbon atoms resulted from the auto combustion of high concentration of biofuel used. " S " values remain constant at 100°C, it begins to increase with temperature. In general, there are several models have been proposed in the literature that describe the ac-conduction mechanism of different types of semiconductors depends on either a mixture of the two processes, quantum mechanical tunnelling or the classical hoping of charges across a potential well. Additionally, it is anticipated that the accountable charge carriers could either be atoms or electrons (or polarons). The SE models explain the behavior of " S

" on temperature and frequency. We can summarize it in the following:

(i) The quantum-mechanical tunneling model (QMT) where the exponent (S) is independent of temperatures. [48].

(ii) the correlated barrier hopping model (CBH) in which s decreases with the increase in temperature [49].

(iii) the overlapping large polar on tunneling (OLPT) model, the exponent s reduces with a rise in temperature to a certain limit after which s upturns with further increase in temperature [50].

(iv) for the non-overlapping small polar on tunneling (NSPT), s found to be strongly temperature dependent and increases with increasing temperature [51&52].

In our study, we found that " S " decreases with the increase in temperature for both S1 and S2. Hence, according to the above mentioned models, the conduction process for these samples can be explained by the CBH model whereas for S3 the most appropriate model to describe the conduction mechanism is the NSPT model.

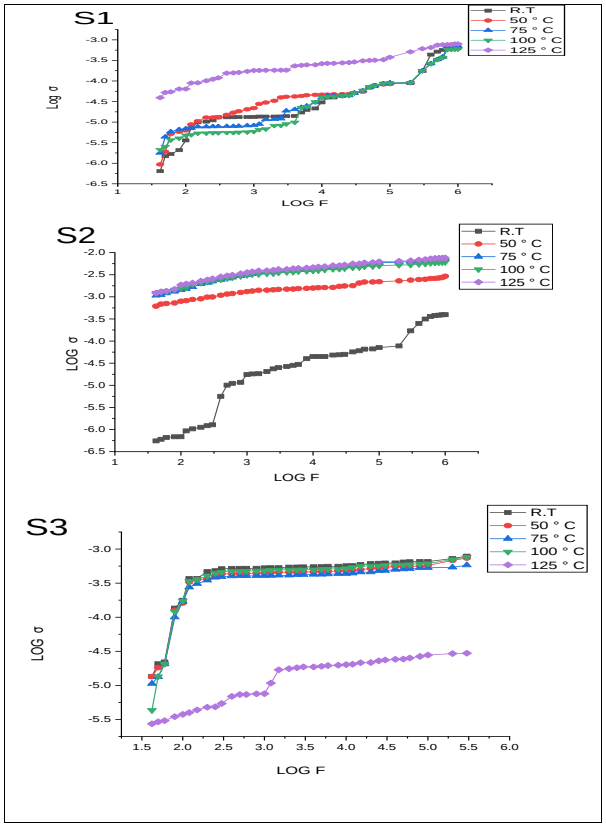

Fig. (4): the variation of Ac-conductivity with frequency at different temperatures for S1, S2 and S3

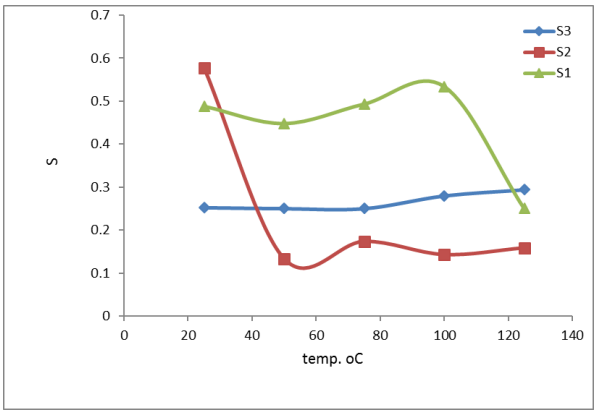

Fig. (5): the variation of " S " with temperature for different samples

3.4.2. DC-Conductivity studies

The dc-Conductivity studies for the temperature dependent (frequency independent) show metal ions hopping between the defect states and is correlated with the band conduction by non-localized carriers with energies greater than the mobility gap. The temperature dependence of dc-electrical conductivity (σ_{dc}) was measured in the temperature range from 25 °C to 125 °C for S1, S2 and S3 samples as shown in Fig. 6. It is clear that σ is temperature dependent and increases as the temperature increased for S1 and S2samples, while S3 sample has a value between both S1 and S2 samples.

For CoMn Ferrites, the electrical conductivity is attributed to the hopping of electrons between the ions of the same element present in different oxidation states. In our samples, the electrons can hop between $Mn^{3+} \rightarrow Mn^{4+}$, $Co^{+1} \rightarrow Co^{+2}$ and $Fe^{+2} \rightarrow Fe^{+3}$ depending upon the distribution of these cations between the octahedral and tetrahedral sites involved in the spinel CoMn Ferrite. The charges can migrate under the influence of the applied field and contribute to the electrical response of the investigated ferrites.

The electrical activation energy was calculated from Arrhenius equation (equation 5), and the values are listed in Table 1.

$$\sigma = \sigma_o \exp(-\Delta Ea/KT) \qquad (5)$$

Where: σ_0 is the Pre-exponential factor, K is the Boltzmann constant, T is the absolute temperature and ΔE_a is the electrical activation energy under the dc fields.

We can conclude from Table 1 that the conduction mechanism for dc-electrical conductivity (σ_{dc}) is electronic in nature for S1 and S2 samples, then the

conduction mechanism converted to ionic conduction as shown in the S3 sample depending upon an increase of C atom due to the high concentration of biofuel.

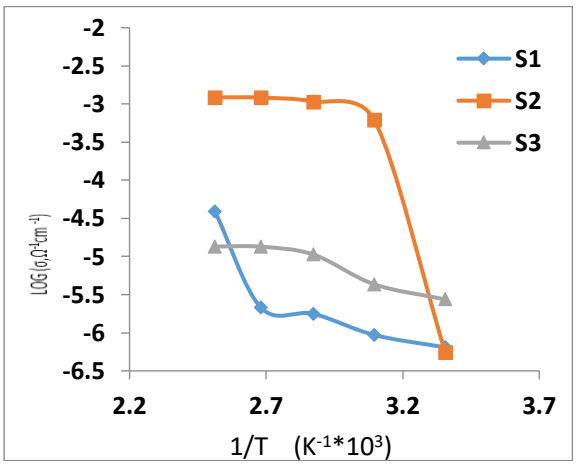

Fig. (6): Variation of dc-electrical conductivity of S1,S2 and S3 samples with 1000/T

3.4.3. frequency dependence of dielectric constant(ε')

Under dielectric studies, we measure the electrical properties of material as a function of frequency at different temperatures. In our experiments the real and imaginary parts of the complex dielectric permittivity, ε* is given by the following equation:

$$\varepsilon^* = \varepsilon - j\varepsilon' \qquad (6)$$

The real part of the dielectric function (dielectric constant, ε′) of S1, S2 and S3 samples was calculated from the measured capacitance at all temperatures and frequencies in according to the following equation:

$$\varepsilon' = (Cd)/(\varepsilon_o A) \qquad (7)$$

Where: C is the capacitance in Farad, d is the thickness in meter, A is the area in m^2, and ε_o is permittivity of free Space ($8.853 \times 10^{-12} Fm^{-1}$).

Fig (7) shows the variation of dielectric constant, ε' , with frequency ranging from 50 Hz to 5 MHz and temperature range from room temperature to 125 °C for S1, S2 and S3 samples. It is obvious that the dielectric constant ε' decreases by increasing of frequency. This decrease is rapid at lower frequencies and become slow at higher frequencies. At certain frequency depending on the concentration of the used biofuel it becomes independent on frequency. Similar results were reported earlier by various authors [53-55].

In fact, there is strong relationship between the dielectric constant ε' and conduction mechanisms. Where the dielectric constant ε' of the investigated ferrites depends upon the hopping of electrons between their cations yielding local movements of these electrons. These local displacement of electrons resulted in dielectric polarization which in turn gives high values of the dielectric constant. Moreover, the presence of magnetic ions of Co, Mn and Fe with their high magnetic moment brought about an increase of these ions at boundaries with subsequent increase in the value of dielectric constant.

Thus, the investigated ferrites have two types of polarization mechanisms at low frequency ranges. The first one is the space charge polarization, while, the second one is the interfacial polarization which arises from different types of defects and a dislocation in the crystal lattice [56]. As shown in Table 1, the as prepared samples have high dielectric constant and these values dependent on the concentration of biofuel.These high values of ε' can be attributed to the formation of magnetic cobalt manganese –iron oxide particles which segregate at the grain boundaries. Hence, the interfacial polarization increases especially at the low frequency region. In addition, the increased values of ε' with increasing biofuel concentration can be attributed to the increase in the carbon atom content that results from the combustion of the egg white.

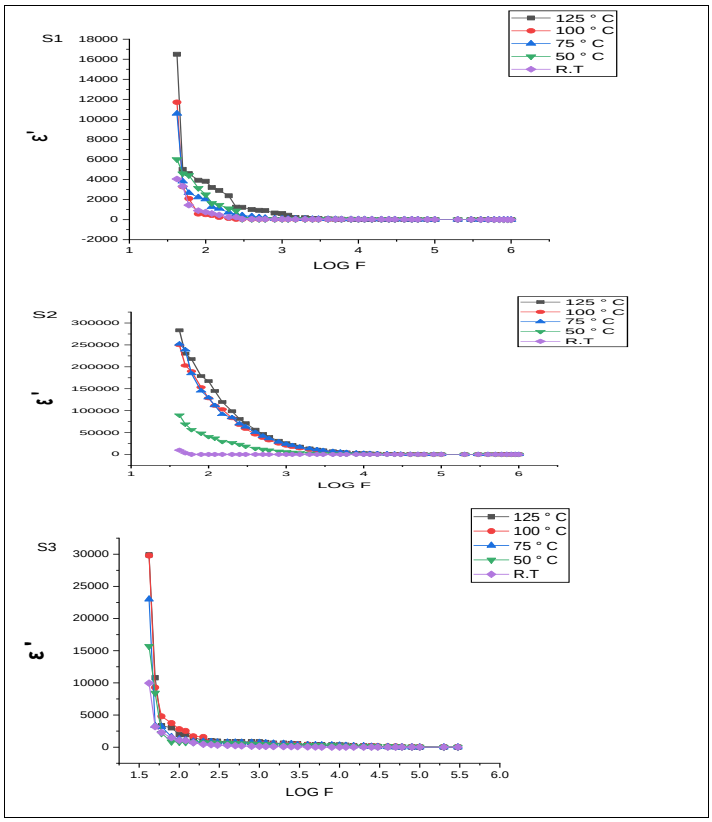

Fig. (7): the variation of dielectric constant with frequency at different temperatures for S1, S2 and S3 samples, respectively.

Samples	σ_{dc}				ΔE_a (eV)		ε'					
	Low temp.		High temp.		Low temp.	High temp.	100 HZ		1kHZ		1MHZ	
							Low temp.	High temp.	Low temp.	High temp.	Low temp.	High temp.
S1	-4.3	-3.1	-4.3	-3.2	0.35	**2.9**	5020	4606	608	24.4	**8.66**	0.49
S2	-4.35	-3.4	-2.9	-2.1	0.24	0.06	10.8	128401	31.2	20407	7.15	18.3
S3	-4.7	-4.5	-3.4	-1.8	0.47	0.007	1050	656	133	46.9	0.25	6.73

Table 1: the values of the electrical conductivity, activation energy and the dielectric constant at high and low temperature ranges of S1, S2 and S3 samples

4. Conclusion

Three samples (S1, S2 and S3) of $Co_{0.3}Mn_{0.7}Fe_2O_4$ nanoparticles were prepared by the egg white assisted combustion method. XRD studies reveal that the prepared samples have a cubic spinel structure. An increase of egg white content resulted in an increase in the crystallinity and abundance of $Co_{0.3}Mn_{0.7}Fe_2O_4$ nanoparticles. The values of band gap energy were calculated from UV–Vis spectra and was found to be 1.4,1.5 and 1.4 eVfor S1, S2 and S3 samples, respectively. TEM image for S2 ensures that their particles are cubic in shape and have particle size ranging from 10 to 15nm.

From the study of ac-electrical conductivity for each sample we determine that the conduction mechanism for S1 and S2 is the overlapping large polaron tunneling (OLPT) where for S3, it is nonoverlapping small polaron tunneling (NSPT).

The electrical activation energy for conduction estimated from Arrhenius plot was found to be 0.352 ,0.244 and 0.476 eV for S1, S3 and S3 samples, respectively, which fits well with the electronic conduction mechanism.

The high values of ε' in the used frequency and temperature ranges were attributed to the formation of magnetic CoMnFe ions at the crystal boundary leading to an increase of the interfacial polarization, especially, at a low frequency. Also, the value of the dielectric constant increased as the concentration of biofuel increased due to an increase of C atoms content.

Declaration:

The authors have no relevant financial or non - financial interests to disclose.

On behalf of all the authors, the corresponding author declares that there is no conflict of interests to the content of this article.

References

[1] J. K Chang and W. T.Tsai, "Material characterization and electrochemical performance of hydrous manganese oxide electrodes for use in electrochemical pseudocapacitors" J. Electrochem. Soc.,(2003),150, A1333-A1338 .

[2] Kuo, S. Liang,Wu and N. Lih"Investigation of pseudocapacitive charge-storage reaction of MnO2.nH2O supercapacitors in aqueous electrolytes" J. Electrochem. Soc., (2006), 153, A1317-A1324 .

[3] K.R.Prasad, andN.Miura"Potentiodynamically deposited nanostructured manganese dioxide as electrode material for electrochemical redox supercapacitors" J. Power Sources,(2004),135, 354 – 360.

[4] K. R. Prasad and N.Miura "Electrochemically synthesized MnO2 – based mixed oxides for high performance redox supercapacitors" Electrochem. Commun,(2004), 6, 1004 – 1008.

[5] M. Toupin, T. Brousse, and D. Belanger "Charge Storage Mechanism of MnO2 Electrode Used in Aqueous Electrochemical Capacitor" Chemistry of Materials,(2004),16, (16) 3184-3190 ,doi:10.1021/cm049649j.

[6] D. Liu, X. Wang, X. Wang, W.Tian, J. liu, C.Zhi, D. He, Y. Bandoand D.Golberg, "Ultrathin nanoporous Fe3O4 – carbon nanosheets with enhanced supercapacitor performance" J. Mater. chem. ,(2013),A, 1, 1952 - 1955.

[7]Y.Wu, and R.Holze"Self- discharge in supercapacitors: causes, effects and therapies: An overview" Electrochem. Energy technical.,(2021), 7, 1-37.

[8]Z.Wang, C.Ma, , H.Wang, Z. Liu, and Z. Hao.,"Facilely synthesized Fe2O3 – graphene nanocomposites as novel electrode materials for supercapacitors with high performance", J. Alloys comp., (2013),552, 486-491 .

[9] B.T.Hanga, I.Watanabea, T.Doi,S.Okada, and J.HYPERLINK

"https://www.sciencedirect.com/science/article/abs/pii/S0378775306011402"Yamaki, "Electrochemical properties of nanosized Fe2O3 loaded carbon as lithium battery anode" J. Power Sources,(2006) ,161,1281-1287 .
[10]S.Ito, K. Ui, N. Koura and K. Akashi "Lithium secondary battery using potassium- β- Ferrites as a new cathode active material' Solid State Ionics"(1998) 113-115, 17- 21 .
[11] J.Sarradim, M. Ribes, A. Guessaus, and K.Elkacemi, "Study of Fe2O3- based thin film electrodes for lithium-ion batteries" Solid State Ionics.,(1998), 112, 35-40 .
[12] N. M. Deraz, A. Alarifi,"Novel processing and magnetic properties of hematite/maghemite nano-particles", Ceramics International,|(2012), 4049-4055ز38
[13] M.V.Reddy, T. Yu,C.H. Sow, Z.X. Shen, C.T. Lim, G.V. Subba Rao and B.V.R.Chowdar, "α-Fe2O3 nanoflakes as an anode material for Li – ion baterries" Adv. Funct. Mater.,(2007),17(15), 2792 – 2799 .
[14] C.Eid, A. Bricude, V.Salles, J.C.Plenet, R. Asmar, Y. Monteily, R. Khoury, A.Khoury and P. Miele,"Iron- based 1D nanostructured by electrospinning process" Nano Technology,(2010) ,21 (12),125701 .
[15] C.T.Cherian, J.M.Kalaivani, P. Ragupathy, P.S. Kumar, V. Thavasi, M.V. Rady, C.H. Sow, S.G. Mhaisalkai, S. Ramakrishma and B.V. Rchowdari, "Electrospun α-Fe2O3 nanorods as a stable, high-capacity anode material for Li-ion batteries" J. Mater.chem.,(2012),22, 12198-12204 .
[16] X.Xia, Q. Hao, W.Lei, W.Wang, D. Sun and X. Wang, "Nanostructured ternary composites of graphene/Fe2O3/polyaniline for high-performance supercapacitors" J. Mater. Chem.,(2012), 22, 16844-16850 .
[17] W.Zheng, Z. Li, H.Zhang, W. Wang, Y. Wang and C.Wang, "Electrospinning route for alpha-Fe2O3 ceramic nanofibers and their gas sensing properties" Mater. Res. Bull., (2009),44,1432- 1436 .
[18] J.Sundaramurthy, P. Suresh Kumar, M. Kalaivani, V. Thavasi, S.G. Mhaisalkara and S.Ramakrishna, "Superior photocatalytic behaviour of novel 1D nanobraid and nanoporous α-Fe2O3 structures" RSC. Adv.,(2012), 2, 8201-8208.
[19] Y.Fan, X.G. Wen, S.H. Yang, and J.G. Lu, " Controlled p- and n-type doping of Fe2O3 nanobelt field effect transistors" Appl. phys. lett.,(2005), 87, 013113 .
[20] Y.Li, Y. Lu, H. Hong, Y. Chen, X. Ma, L. Guo, Z. Wang, J. Chen, M. Zhu, J. Ni, H. Gu, J. Lu, and J.Y. Ying, " Synthesis of Pt@Fe2O3nanorods as MRI probes for in vivo application" Chem. Commun.,(2001), 47(22),6320- 6322 .
[21] G.Wang, L. Zhang and J.Zhang, "A Review of Electrode Materials for Electrochemical Supercapacitors" Chem. Soc. (2012), Rev., 41(2), 797-828 .
[22] K.K.Lee, S. Deng, H.M Fan, R.S. Mhaisalka ,H.R. Tan, E.S. Tok, K.P. Loh, W.S. Chin and C.H. Sow, "α-Fe2O3 nanotubes-reduced graphene oxide composites as synergistic electrochemical capacitor materials" Nanoscale, (2012),4(9),2958 -2961.
[23]T.C.Liu, W.G. Pell and B.E.Canway, "Stages in the development of thick cobalt oxide films exhibiting reversible redox behavior and pseudocapacitance" Electrochimica. Acta, (1999),44(17) 2829- 2842.
[24]H.K.Kim, T.Y. Senog, J.H. Lim, W.L. Cho and Y.S. Yoem, "Electrochemical and structural properties of radio frequency sputtered cobalt oxide electrodes for thin-film supercapacitors" J. Power Sources,(2001),102 (1-2) 167 – 171 .
[25] V.Srinivasam and J.W. Weidner, "Capacitance studies of cobalt oxide films formed via electrochemical precipitation" J. Power Sources,(2002), 108(1-2) 15- 20 .
[26] C.Lin, J.A.Ritter and B.N.Popov, " Characterization of Sol-Gel-Derived Cobalt Oxide Xerogels as Electrochemical Capacitors" J. Electrochem. Soc.,(1998),145, 4097 .
[27]V.R.Shinde, S.B. Mahadik, T.P. Gujar and C.D.Lokhande, "Supercapacitive cobalt oxide (Co3O4) thin films by spray pyrolysis" Appl. Surf. Sci.,(2006),252(20) 7487- 4892 .
[28] S.G.Kandalkar, C.D. Lokhande, R.S. Mane and S.H.Hau, "A non-thermal chemical synthesis of hydrophilic and amorphous cobalt oxide films for supercapacitor application" Appl. Surf. Sci.,(2007),253 (8), 3952- 3956 .
[29]J.K.Chang, U.C.Hsieh and W.T. Tssai, " Effects of the Co content in the material characteristics and supercapacitive performance of binary Mn–Co oxide electrodes" J. Alloys and Compound,2008,461 (1-2) 667-674 .
[30]V.Gupta, S.Gupta, and N.Himra, "Potentiostatically deposited nanostructured CoxNi1−x layered double hydroxides as electrode materials for redox-supercapacitors" J. Power Sources,(2008),175, 680 -685 .
[31]K.Chang, M.T. Lee, C.H. Huang and W.T. Tsai, " Physicochemical properties and electrochemical behavior of binary manganese–cobalt oxide electrodes for supercapacitor applications" Mater. Chem. Phys.,(2008),108(1), 124- 131.
[32]X.He,Y. Zhao, R. Chen, H. Zhang, J. Liu, Q. Liu, D. Song, R. Lian, and J.Wang, " Hierarchical FeCo2O4@polypyrrole core/shell nanowires on carbon cloth for high – performance flexible All – Solid State asymmetric supercapacitors" ACS sustainable Chem. Eng.,(2018),6(11), 1445- 1454 .
[33]S.Zhang, B.YIN, C. Liu, Z. Wang, and D.Gu, "Self-assembling hierarchical NiCo2O4/MnO2 nanosheets and MoO3/PPy core-

shell heterostructured nanobelts for supercapacitor" Chem. Eng. J.,(2017),312, 296-305 (2017).
[34] L.Huang, D.Chen, Y. Ding, S. Feng, Z. Wang, and M.Liu, "Nickel-cobalt hydroxide nanosheets coated on NiCo2O4 nanowires grown on carbon fiber paper for high-performance pseudocapacitors" Nano Lett.,(2013),13, 3135-3139 .
[35] S.Chem, M. Xue, Y. Pam, L. Zhu and S.Qiu, "Rational design and synthesis of NixCo3−xO4 nanoparticles derived from multivariate MOF-74 for supercapacitors" J. Mater. Chem. (2015),A, ,3 (40), 20145-20152 .
[36]N. M. Deraz, "Glycine-assisted fabrication of nanocrystalline cobalt ferrite system", Journal of Analytical and Applied Pyrolysis, (2010), 88 103–109.
[37]M.Cernea, P. Galizia, I.Ciuchi, G. Aldica, V. Mihalache, L. Diamandescu, and C.Galassi"CoFe2O4 magnetic ceramic derived from gel and densified by spark plasma sintering" J. Alloys Compd.,(2016),656, 854-862 .
[38]X.Yang, X. Wang, and Z.Zhang, Z. "Electrochemical properties of submicron cobalt ferrite spinel through co-precipitation method", J. Cryst. Growth, (2005),277 467-47.
[39] N. M. Deraz, "Facile and eco-friendly route for green synthesis of magnesium ferrite nano particles" Science of Sintering, (2020),52(1),53-65.
[40]L.Yao, Y. Xi, G. Xi, and Y.Feng, " Synthesis of cobalt ferrite with enhanced magnetostriction properties by the sol−gel−hydrothermal route using spent Li-ion battery" J. Alloys Compd.,(2016),680, 73 - 79 https://doi.org/10.1016/j.jallcom.2016.04.092.
[41]A.Kalam, A.G. Al-Sehemi, M. Assiri, G. Du, T. Ahmad, I. Ahmad, M.Pannipara, "Modified solvothermal synthesis of cobalt ferrite (CoFe2O4) magnetic nanoparticles photocatalysts for degradation of methylene blue with H2O2/visible ligth" Results Phys.,(2018)8,1046-1053 , https://doi.org/10.1016/j.rinp.2018.01.045.
[42]J.Tauc "Optical properties and electronic structure of amorphous Ge and Si" . Materials Research Bulletin.(1968), 3, 37–46. doi:10.1016/0025-5408(68)90023-8
[43]B.J.Raja, M.R. Yadav, V.P. Manjari, B. Babu, C.R. Krishna, R.V.S.S.N Ravikuiar, "Synthesis and characterization of undoped and Mn(II)ions doped Li2CaAl4(PO4)4F4 nanophosphors" J. Mol. Struct.(2014), 1076, 461-46 .
[44]M.A.L.Nobre and S.Lanfredi, "AC conductivity and conduction mechanism of NaNbO3 semiconductor antiferroelectric ceramic:A relaxational approach at high temperature" Appl. Phys. lett.,(2003), 83,3102 .
[45]A.Rado, D. Łukowiec, M. Kremzer, J. Mikuła and P.Włodarczyk"Electrical Conduction Mechanism and Dielectric Properties of Spherical Shaped Fe3O4 Nanoparticles Synthesized by Co-Precipitation Method" Materials, (2018),11, 735 ; doi:10.3390/ma11050735
[46]E.Kadri, K. Dhahri, A. Zaafouri, M. Krichen, M. Rasheed, K. Khiroouni, R. Barille "Ac conductivity and dielectric behavior of a-Si : H/C-Si 1-yGey/P-Si thin films synthesized by molecular beam epitaxial method" J. Alloys. Comp.,(2017),705, 708-713 .
[47]Abdel-Karim, M.Aml ,A.H. Salama and L.Hassan Mohammad "Electrical conductivity and dielectric properties of nanofibrillated cellulose thin films from bagasse" J. Phys. Org. Chem.,(2018), e3851 .
[48]R.Punia, R.S.Kundu, M. Dutt, S. Muxen gavel, and N.Kishorc, "Temperature and frequency dependent conductivity of bismth zinc vanadate semiconducting glassy systems" J. Appl. phys.,(2012),112, 083701 .
[49]S.M.Barchani and M.Megdiche "Electrical properties and conduction mechanism in the NaLaMnMoO6 double perovskite ceramic" J. Phy. Chem. Solids, (2018),114, 121-128 .
[50]M.Tan, Y. Koseoglu, F. Alana and E.Senturk "Overlapping large polaron tunneling conductivity and gaint dielectric constant in Ni0.6Zn0.5Fe1.5Cr0.5O4 nanoparticles (NPS) " J. Alloys Comp., (2011),509, 9399-9405 .
[51]A.Bemal, B.M.G. Melo, P.R. Prezas, M. Bejar, E. Dhahr, M.A. Valente, M.P.F. Graca, B.A.Nagueira and B.F.O Costa " structural, morphological, roman and ac-electrical properties of the multiferroic sol. gel made Bi0.8Er0.1 Ba0.1Fe0.96Cr0.02Co0.2O3 material" J. Alloys. Comp.,(2019),775, 304-315 .
[52]H.Rahmoui, M. Nouiri, R.Jemai, N.Kallel, F. Rzigua, A. Selmi, K. Khirouni and S.Alaya, "Electrical conductivity and complex impedance analysis of 20% Ti-doped La0.7Sr0.3MnO3 perovskite" J. Magn. Magn. Mater., (2007),316, 23-28 .
[53]J.lott, , C.Xia, L. Kosmosky, C. Weder, J. sham, "Terahertz photonic crystals based on barium titanate/polymer nanocomposites" Adv. Mater., (2008),20 (19), 3649 – 3653 (2008).
[54] M.L.Hassan, A.F. Ali, A.H. Salama, and A.M.Abdel. Karim, " Novel cellulose nanofibers/barium titanate nanoparticles nanocomposites and their electrical properties" J. Phys. Org. Chem.,(2019),32, e3897 .
[55] S.C.Watawe, B.D. Sutar, and B.K.Chougule, "Microstructure, frequency and temperature-dependent dielectric properties of cobalt-substituted lithium ferrites" J. Magn. Magn. Mater., (2009),214, 55- 60 (2009).
[56]C.Mu, N. chem, X. Pan, X. Shen, and X.Gu, , "Preparation and microwave absorption properties of barium ferrite nanorods" Mater. Lett., (2008),62 (6-7), 840- 842.